1

# Chirality in Astrophysics

Axel Brandenburg

*Nordita, KTH Royal Institute of Technology and Stockholm University, and*
*The Oskar Klein Centre, Department of Astronomy, Stockholm University, Stockholm, Sweden*
*\*E-mail: brandenb@nordita.org, May 6, 2022, Revision: 1.65*
*https://www.nordita.org/~brandenb*

Chirality, or handedness, enters astrophysics in three distinct ways. First, magnetic field and vortex lines tend to be helical and have a systematic twist in the northern and southern hemispheres of a star or a galaxy. Helicity is here driven by external factors. Second, chirality can also enter at the microphysical level and can then be traced back to the parity-breaking weak force. Third, chirality can arise spontaneously, but this requires not only the presence of an instability, but also the action of nonlinearity. Examples can be found both in magnetohydrodynamics and in astrobiology, where homochirality among biomolecules probably got established at the origin of life. In this review, all three types of chirality production will be explored and compared.

*Keywords*: Magnetic helicity; chiral magnetic effect; gravitational waves; homochirality

## 1. Introduction

Chirality, or handedness, plays important roles in many different fields of astrophysics, including astrobiology. There are three distinct types of chirality production: (i) driven chirality due to external factors, (ii) driven chirality due to intrinsic properties, and (iii) spontaneous chirality production due to instability and nonlinearity. The primary applications for these three types of chirality production are rather distinct, but one can find unifying circumstances under which the different types can be demonstrated and compared. One such circumstance is given by the presence of magnetic fields.

Magnetic fields can experience twisting that makes them helical, but the central question is what determines the sign of this twist—especially if it is a systematic one, always being in the same sense. When there are extrinsic or intrinsic factors such as the combination of rotation and stratification in a star, or intrinsic factors such as the presence of fermions of one of two handednesses, the answer is in principal clear. However, there can also be spontaneous helicity production, where the sign depends ultimately on chance, so both signs are possible under almost identical conditions. An example that we discuss at the end of this review is in the field of magnetohydrodynamics (MHD), where a magnetic field in a stratified atmosphere that exhibits a magnetic buoyancy instability where, in the end, once nonlinearity plays a role, one particular handedness dominates to nearly hundred percent. It is this example that, in a broad sense, also carries over to astrobiology and the origin of life, where one particular chirality of biomolecules eventually dominates

2

Table 1.    Summary of three types of chirality production in astrophysics.

| What | Where | How |
| --- | --- | --- |
| Helicity, driven by stratification & rotation | stars, planets, galaxies | magnetic field from Zeeman effect, polarization, in situ in solar wind |
| Fermion asymmetry, axions | entire universe | polarization patters, photon arrival direction statistics, circularly polarized gravitational waves |
| Spontaneous chirality production | astrobiology, MHD | enantiospecific uptake of nutrients |

and leads, to what is known as homochirality. Magnetic fields are probably not involved in the origin of life, but there are simple mathematical analogies in both cases.

In Table 1, we summarize the three types of chirality production under the "what" column or category. The "where" category lists some specific examples, and the "how" category highlights some specific techniques for measuring chirality for those three types.

We begin with some historical remarks highlighting the significance of helicity of magnetic fields (Sect. 2). In Sects. 3–5, we discuss aspects of the three types in more detail and then conclude in Sect. 6 with some additional reflections. We emphasize that we use the terms chirality, helicity, and handedness rather interchangeably, although technically this is not always accurate.

## 2. Historical remarks

### 2.1. *Helicities in fluid dynamics and MHD*

In the context of fluid dynamics, the term helicity was coined by H. Keith Moffatt,[1] who identified the topological equivalence between the knottedness of vortex lines in fluid dynamics and the kinetic helicity. In fact, the term helicity was already used by Robert Betchov[2] in 1961, but Moffatt proposed this name in his 1969 paper on the grounds that this term is also used in subatomic physics to describe the alignment or anti-alignment of spin and momentum of fermions, for example. Mathematically, the mean kinetic helicity density is defined as $\langle \boldsymbol{\omega} \cdot \boldsymbol{u} \rangle$, where the vorticity $\boldsymbol{\omega} = \boldsymbol{\nabla} \times \boldsymbol{u}$ is the curl of the velocity $\boldsymbol{u}$. Kinetic helicity is a pseudoscalar, i.e., it changes its sign when the system is inspected through a mirror. Likewise, $\boldsymbol{\omega}$ is a pseudovector, so it is more meaningful to plot it with its sense of rotation (which changes in a mirror), rather than a vector with an arrow at its end.

In the magnetic context, the corresponding quantity that we now call magnetic helicity was already studied by Lodewijk Woltjer[3] in 1958 to characterize force-free magnetic fields and by John Bryan (J.B.) Taylor[4] in 1974 to describe the relaxation of a toroidal plasma.
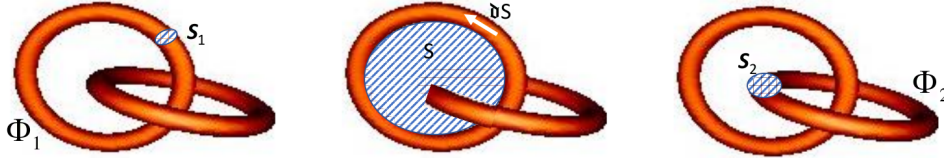
Fig. 1.  Illustration showing that the line integral $\oint_{\partial S} \boldsymbol{A} \cdot \mathrm{d}\boldsymbol{\ell}$ along flux tube $\Phi_1$, can be written as a surface integral over the enclosed surface $S$, $\int_S (\boldsymbol{\nabla} \times \boldsymbol{A}) \cdot \mathrm{d}\boldsymbol{S}$, where $\partial S$ is the line along flux tube $\Phi_1$. However, the only nonvanishing contribution comes from flux tube $\Phi_2$, i.e., $\int_{S_2} \boldsymbol{B} \cdot \mathrm{d}\boldsymbol{S}$.

## 2.2. *Magnetic helicity conservation*

The quantities that we shall focus on here are mainly the mean magnetic helicity density $\langle \boldsymbol{A} \cdot \boldsymbol{B} \rangle$, where $\boldsymbol{B} = \boldsymbol{\nabla} \times \boldsymbol{A}$ is the magnetic field expressed in terms of its vector potential $\boldsymbol{A}$, and the magnetic helicity over a volume containing two interlocked flux loops, $\int_{V_1+V_2} \boldsymbol{A} \cdot \boldsymbol{B} \, \mathrm{d}V = \int_{V_1} \boldsymbol{A} \cdot \boldsymbol{B} \, \mathrm{d}V + \int_{V_2} \boldsymbol{A} \cdot \boldsymbol{B} \, \mathrm{d}V$. The volumes $V_1$ and $V_2$ are those of the two tubes. For $V_1$, we can split the volume integral into a line integral $\oint_{\partial S} \boldsymbol{A} \cdot \mathrm{d}\boldsymbol{\ell}$ along the flux tube and a surface integral $\int_{S_1} \boldsymbol{B} \cdot \mathrm{d}\boldsymbol{S}$ across the tube, i.e.,

$$\int_{V_1} \boldsymbol{A} \cdot \boldsymbol{B} \, \mathrm{d}V = \left( \int_{S_1} \boldsymbol{B} \cdot \mathrm{d}\boldsymbol{S} \right) \left( \oint_{\partial S} \boldsymbol{A} \cdot \mathrm{d}\boldsymbol{\ell} \right); \tag{1}$$

see Figure 1. Using Stokes' theorem, the line integral along tube 1 can be rewritten as a surface integral over the magnetic field going through the flux ring, but its only nonvanishing contribution comes from the other intersecting tube with surface $S_2$. Thus, we have $\int_{V_1} \boldsymbol{A} \cdot \boldsymbol{B} \, \mathrm{d}V = \pm \Phi_1 \Phi_2$, and likewise for $V_2$, so we get a factor 2. The sign depends on the relative orientation of the field vectors in the two tubes, so we write here $\int \boldsymbol{A} \cdot \boldsymbol{B} \, \mathrm{d}V = \pm 2\Phi_1 \Phi_2$.

The magnetic field is a pseudovector. Its evolution is governed by the homogeneous Maxwell equation $\partial \boldsymbol{B}/\partial t = -\nabla \times \boldsymbol{E}$, where $t$ is time and $\boldsymbol{E}$ is the electric field. Since $\boldsymbol{\nabla} \cdot \boldsymbol{B} = 0$, it is convenient to consider the uncurled induction equation

$$\partial \boldsymbol{A}/\partial t = -\boldsymbol{E} - \boldsymbol{\nabla}\phi, \tag{2}$$

where $\phi$ is the electric (or scalar) potential. To obtain an evolution equation for $\boldsymbol{A} \cdot \boldsymbol{B}$, we compute $\boldsymbol{A} \cdot \dot{\boldsymbol{B}} + \dot{\boldsymbol{A}} \cdot \boldsymbol{B}$, where dots denote partial time differentiation, and find

$$\frac{\partial}{\partial t}(\boldsymbol{A} \cdot \boldsymbol{B}) = -2\boldsymbol{E} \cdot \boldsymbol{B} - \boldsymbol{\nabla} \cdot \underbrace{(\phi \boldsymbol{B} + \boldsymbol{E} \times \boldsymbol{A})}_{\text{helicity flux}}. \tag{3}$$

We see that the magnetic helicity production depends on $\boldsymbol{E} \cdot \boldsymbol{B}$ and on the presence of magnetic helicity fluxes, $\boldsymbol{\mathcal{F}}_H = \phi \boldsymbol{B} + \boldsymbol{E} \times \boldsymbol{A}$. The $\boldsymbol{E} \cdot \boldsymbol{B}$ term plays important roles in electrically non-conducting environments, for example during inflation in the early universe when space-time became extremely diluted. By contrast, in the contemporary universe, and even in the space between galaxy clusters, there is still

4

sufficient conductivity so that the laws of MHD apply, and not the vacuum equations for electromagnetic waves, which apply during inflation. In MHD, the electric field is given by $\boldsymbol{E} = -\boldsymbol{u} \times \boldsymbol{B} + \boldsymbol{J}/\sigma$, where $\boldsymbol{J}$ is the current density and $\sigma$ the electric conductivity. We see that the first term does not contribute to $\boldsymbol{E} \cdot \boldsymbol{B}$. Thus, the only contribution comes from $\boldsymbol{J} \cdot \boldsymbol{B}/\sigma$, so we have

$$\frac{\partial}{\partial t}\langle \boldsymbol{A} \cdot \boldsymbol{B} \rangle = -2\eta \langle \boldsymbol{J} \cdot \boldsymbol{B} \rangle, \tag{4}$$

where $\eta = (\mu_0 \sigma)^{-1}$ is the magnetic diffusivity, and angle brackets denote volume averaging. When the conductivity is large, $\eta$ is small, and $\eta \langle \boldsymbol{J} \cdot \boldsymbol{B} \rangle$ converges to zero like $\eta^{1/2}$ as $\eta \to 0$.

The smallness of $\eta$ in many astrophysical settings makes $\langle \boldsymbol{A} \cdot \boldsymbol{B} \rangle$ nearly perfectly conserved,[3] except for the presence of magnetic helicity fluxes. Those vanish in homogeneous systems (e.g., in homogeneous helical turbulence), but astrophysical dynamos are usually not homogeneous and magnetic helicity fluxes, for example out of the star or between its northern and southern hemispheres, are believed to play important roles in astrophysical dynamos to alleviate some serious constraints[5] arising from the magnetic helicity conservation otherwise.

### 2.3. *Helicity-driven large-scale dynamos*

To understand the aforementioned constraint, we need to emphasize that magnetic helicity is usually connected with the presence of kinetic helicity, $\langle \boldsymbol{\omega} \cdot \boldsymbol{u} \rangle$. It can lead to an electromotive force along the mean magnetic field, $\overline{\boldsymbol{B}}$, of the form

$$\overline{\boldsymbol{u} \times \boldsymbol{b}} = \alpha \overline{\boldsymbol{B}} - \eta_{\text{t}} \mu_0 \overline{\boldsymbol{J}}, \tag{5}$$

where $\boldsymbol{u} = \boldsymbol{U} - \overline{\boldsymbol{U}}$ and $\boldsymbol{b} = \boldsymbol{B} - \overline{\boldsymbol{B}}$ are fluctuations of velocity and magnetic fields, and $\overline{\boldsymbol{J}} = \boldsymbol{\nabla} \times \overline{\boldsymbol{B}}/\mu_0$ is the mean current density. Here, overbars denote averaging (for example planar or $xy$ averaging), but the type of averaging depends on the particular problem. Under the assumption of isotropy and high conductivity,[6] we have $\alpha = -\langle \boldsymbol{\omega} \cdot \boldsymbol{u} \rangle \tau/3$ and $\eta_{\text{t}} = \langle \boldsymbol{u}^2 \rangle \tau/3$, and $\tau$ is the correlation time. The $\alpha \overline{\boldsymbol{B}}$ term can lead to an exponential growth of $\overline{\boldsymbol{B}}$. The second term just leads to an enhancement of the microphysical magnetic diffusion, $\eta \mu_0 \overline{\boldsymbol{J}}$.

The $\alpha$ effect leads to the generation of magnetic helicity of the mean field with $\overline{\boldsymbol{A}} \cdot \overline{\boldsymbol{B}} = O(\overline{\boldsymbol{B}}^2/k_{\text{m}}) \neq 0$, where $k_{\text{m}}$ is the typical wavenumber of the magnetic field. However, since the total magnetic helicity is conserved (and vanishing of the field was very small initially), we must generate small-scale magnetic helicity, $\langle \boldsymbol{a} \cdot \boldsymbol{b} \rangle$, of opposite sign. The resulting current helicity, $\langle \boldsymbol{j} \cdot \boldsymbol{b} \rangle \approx k_{\text{f}}^2 \langle \boldsymbol{a} \cdot \boldsymbol{b} \rangle$, with some typical wavenumber $k_{\text{f}}$ characterizing the fluctuation scales, quenches the $\alpha$ effect and leads to slow dynamo saturation.[7]

We will not go into further details here, but refer the reader to reviews on the subject.[5,8] This field of research remains very active and there are still important questions regarding magnetic helicity fluxes that remain controversial.

## 3. Chirality driven by external factors

### 3.1. *Examples of helicities: even and odd in B*

We discuss here three different helicities: kinetic helicity $\langle \boldsymbol{\omega} \cdot \boldsymbol{u} \rangle$, magnetic helicity $\langle \boldsymbol{A} \cdot \boldsymbol{B} \rangle$, and cross helicity $\langle \boldsymbol{u} \cdot \boldsymbol{B} \rangle$. The latter reflects the linkage between an $\boldsymbol{\omega}$ tube (vortex tube) and a $\boldsymbol{B}$ tube (magnetic flux tube). To understand the production of kinetic helicity, one has to realize that it is a pseudoscalar. This means, that it is the product of a polar vector and an axial vector. Rotation, for example, is an axial vector, but that alone cannot produce magnetic or kinetic helicity. However, in the presence of both rotation $\boldsymbol{\Omega}$ and gravitational stratification characterized by the gravitational acceleration $\boldsymbol{g}$, which is a polar vector, we can produce the pseudoscalar $\boldsymbol{g} \cdot \boldsymbol{\Omega}$. Thus, kinetic helicity can be produced if one can identify external factors such as the combined presence of $\boldsymbol{g}$ and $\boldsymbol{\Omega}$ that could explain the presence of a non-vanishing helicity. However, these external factors must also be even in the magnetic field, so a nonvanishing $\langle \boldsymbol{u} \cdot \boldsymbol{B} \rangle$ with a systematic sign cannot be explained in that way. Finite cross helicity can, however, be explained if rotation was replaced by an imposed magnetic field $\boldsymbol{B}_0$, so that $\boldsymbol{g} \cdot \boldsymbol{B}_0$ would be finite.

We thus see that $\langle \boldsymbol{\omega} \cdot \boldsymbol{u} \rangle$ may be linked to $\boldsymbol{g} \cdot \boldsymbol{\Omega}$, although this needs to be (and has been) verified using a detailed calculation.[6] In spherical coordinates $(r, \theta, \phi)$, where $\theta$ is colatitude and the unit vectors of $\boldsymbol{g}$ and $\boldsymbol{\Omega}$ are $\hat{\boldsymbol{g}} = (-1, 0, 0)$ and $\hat{\boldsymbol{\Omega}} = (\cos\theta, -\sin\theta, 0)$, respectively, we have $\boldsymbol{g} \cdot \boldsymbol{\Omega} = -\cos\theta$, which is negative in the north and positive in the south. This is indeed consistent with the observed sign of $\langle \boldsymbol{\omega} \cdot \boldsymbol{u} \rangle$, and it is also found to govern the sign of the magnetic helicity, but only at small and moderate length scales, i.e., $\langle \boldsymbol{a} \cdot \boldsymbol{b} \rangle$.

Regarding the cross helicity, there is indeed a systematic large-scale magnetic field $\boldsymbol{B}_0$ at the solar surface, although there can be several sign changes in each hemisphere. (The radius of the Sun is $700\,\mathrm{Mm}$, and $1\,\mathrm{Mm} = 1000\,\mathrm{km}$, a useful unit in solar physics!) On smaller scales of $\geq 20\,\mathrm{Mm}$, it also changes between the two sides of a sunspot pair, which is consistent with observations.[9] It turns out that $\langle \boldsymbol{u} \cdot \boldsymbol{B} \rangle \approx -(\eta_{\mathrm{t}}/c_{\mathrm{s}}^2)\, \boldsymbol{g} \cdot \boldsymbol{B}_0$, where $\eta_{\mathrm{t}}$ is the turbulent magnetic diffusivity and $c_{\mathrm{s}}$ is the sound speed.[10] This production mechanism of cross helicity may play a role in theories of shallow sunspot formation.[11,12]

### 3.2. *Observing helicity*

#### 3.2.1. *Measuring magnetic helicity from solar magnetograms*

Above the surface of the Sun, one often sees twisted structures in extreme ultraviolet and x-ray images, which are suggestive of helicity.[13–15] Even space observations of the surface of the Earth reveal cyclonic cloud patterns that have opposite orientation in the northern and southern hemispheres. However, to draw a connection with magnetic helicity, one must first detect the magnetic field. This is possible through the Zeeman effect, which causes circular polarization proportional to the line-of-sight magnetic field, and linear polarization related to the perpendicular magnetic

6

field component – except for a $\pi$ ambiguity, which means that polarization measurements are never able to tell where the tip of the magnetic field vector is, so there is an uncertainty with respect to $180°$. For strong enough magnetic fields, a "disambiguation procedure" based on a minimal magnetic energy assumption allows one to determine the full $\boldsymbol{B}$ vector at the solar surface.[16,17] However, there is still not enough information about the changes of polarization parameters along the line of sight, i.e., below and above the surface of the Sun.

To make progress, one has to make some extra assumptions. One possibility is to determine just the components normal to the surface, $B_\parallel \equiv B_z$ and $J_\parallel \equiv J_z = \partial_x B_y - \partial_y B_x$, where local Cartesian coordinates $(x, y, z)$ have been employed, and compute $J_\parallel B_\parallel$. This was first done by Seehafer,[18] who found that $J_\parallel B_\parallel$ is negative in most of the active regions in the northern hemisphere of the Sun, and positive in most of the active regions in the southern one. From $J_\parallel$ and $B_\parallel$, one can also determine a proxy of the magnetic helicity spectra, $\tilde{A}_\parallel(\boldsymbol{k}_\perp)\tilde{B}_\parallel^*(\boldsymbol{k}_\perp)$, where tildes denote Fourier transformation, $\boldsymbol{k}_\perp$ is the wavevector in the horizontal ($xy$ surface) plane, and the asterisk denotes the complex conjugate. Here, $\tilde{A}_\parallel = \tilde{J}_\parallel/\boldsymbol{k}_\perp^2$. This has been done[19,20] and magnetic energy and helicity spectra are shown in Figure 2(a) for active region AR 11158. Subsequent work[9] also presented cross helicity spectra.

### 3.2.2. *Magnetic helicity spectra from a time series*

A completely different approach, due to Matthaeus and et al.,[21] which also makes use of Fourier transformation, is to use *in situ* observations of time series of the $\boldsymbol{B}$ vector in the solar wind at one point in space. One can then make use of what is known as the Taylor hypothesis to associate the temporal changes with different positions through $\boldsymbol{r} = \boldsymbol{r}_0 - \boldsymbol{v}t$, where $\boldsymbol{v}$ is the velocity vector of the solar wind, and $\boldsymbol{r}_0$ is a reference position. Assuming homogeneity, i.e., that the statistical properties are independent of position, one can write the magnetic two-point correlation tensor in Fourier space as

$$4\pi\langle\tilde{B}_i(\boldsymbol{k})\tilde{B}_j(\boldsymbol{k})\rangle = (\delta_{ij} - \hat{k}_i\hat{k}_j)2\mu_0 E_{\mathrm{M}}(k) - \mathrm{i}\epsilon_{ijk}\hat{k}_k H_{\mathrm{M}}(k), \tag{6}$$

where $E_{\mathrm{M}}(k)$ is the magnetic energy spectrum, normalized such that $\int E_{\mathrm{M}}(k)\,\mathrm{d}k = \langle\boldsymbol{B}^2\rangle/2\mu_0$, and $H_{\mathrm{M}}(k)$ is the magnetic helicity spectrum with $\int H_{\mathrm{M}}(k)\,\mathrm{d}k = \langle\boldsymbol{A}\cdot\boldsymbol{B}\rangle$. This procedure revealed a clear hemispheric antisymmetry with respect to the solar equator.[22]

Comparing Figure 2(a) and (b), which are here both for the southern hemisphere, we see that at the solar surface, $H_{\mathrm{M}}(k)$ has the expected sign at small and intermediate scales ($k > 0.1\,\mathrm{Mm}^{-1}$). In the solar wind,[a] however, a positive sign is only seen at very large scales ($k < 30\,\mathrm{AU}^{-1} \approx 0.0002\,\mathrm{Mm}^{-1}$). The typical wavenumber at which the spectral helicity changes sign at the solar surface (radius $700\,\mathrm{Mm}$) is $k \approx 0.1\,\mathrm{Mm}^{-1}$. Expanding this linearly to a distance of 1 AU yields a

---

[a]The mean distance between the Sun and the Earth is one astronomical unit (1 AU $\approx 149,600\,\mathrm{Mm}$).
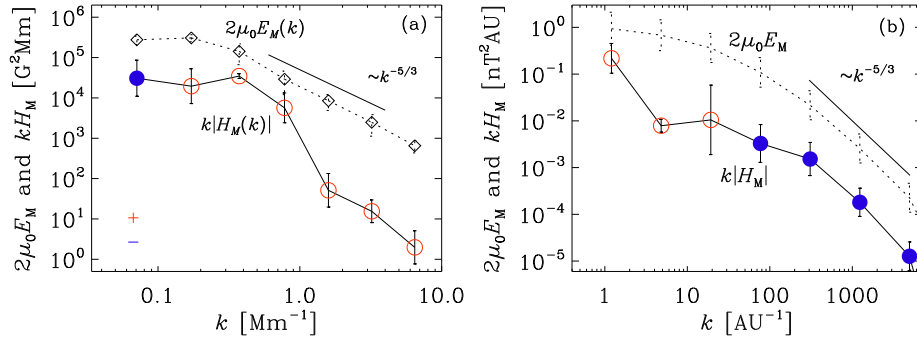
Fig. 2.    Magnetic energy and magnetic helicity spectra for southern latitudes (a) at the solar surface in active region AR 11158, and (b) in the solar wind at $\sim 1\,\mathrm{AU}$ distance ($1\,\mathrm{AU} \approx 149{,}600\,\mathrm{Mm}$). Positive (negative) signs are shown as red open (blue filled) symbols. Positive signs are the solar surface at intermediate and large $k$ correspond to positive values in the solar wind at small $k$. Note that $1\,\mathrm{G} = 10^{-4}\,\mathrm{T} = 10^5\,\mathrm{nT}$.

corresponding wavenumber of $k = 70\,\mathrm{AU}^{-1}$, which is indeed where the spectrum in the solar wind changes sign; see Figure 2(b). However, the change is here the other way around: from positive to negative at large $k$. The reason for this sign mismatch is not yet fully understood, but it is worth noting that a sign reversal has also been seen in idealized numerical simulations of stellar and galactic dynamos embedded in a turbulent exterior.[23–25] Chiral solar wind MHD turbulence has also been studied in the equatorial plane, but then both signs of helicity are possible.[26,27] Both signs of magnetic helicity have also been found from multi-spacecraft measurements in close proximity of the equatorial plane.[28]

### 3.2.3.  Canceling Faraday depolarization with helicity

There is an intriguing possibility to determine magnetic helicity from the cancelation of Faraday depolarization.[29,30] It might be particularly suitable for calculating the magnetic helicity in the outskirts of edge-on galaxies, where one might see the sign of magnetic helicity being reversed.

Normally, in the absence of magnetic helicity, Faraday rotation causes Faraday depolarization. This is caused by the superposition of different polarization planes from different depths along the line of sight. At the same time, however, the perpendicular component of the magnetic field itself can rotate about the line of sign if it is helical. These two effects can then either enhance each other (and make the Faraday depolarization more complete), or they can offset each other and lead to increased transmission or reduced depolarization.

Mathematically, this can be seen by considering the observable polarization,

8

written in complex form as

$$P(x, z, \lambda^2) \equiv Q + \mathrm{i}U = p_0 \int_{-\infty}^{\infty} \epsilon \, e^{2\mathrm{i}(\psi_P + \phi\lambda^2)} \, \mathrm{d}y, \tag{7}$$

where $\psi_P = \psi_B + \pi/2$ is the electric field angle, $\psi_B = \mathrm{atan}(B_y, B_x)$ is the magnetic field angle, $\epsilon(x, y, z)$ is the emissivity, $p_0$ is the degree of polarization, $\lambda$ is the wavelength,

$$\phi(x, y, z) = -K \int_{-\infty}^{y} n_{\mathrm{e}}(x, y', z) \, B_{\parallel}(x, y', z) \, \mathrm{d}y' \tag{8}$$

is the Faraday depth, with $n_{\mathrm{e}}$ being the electron density and $K = 0.81 \, \mathrm{m}^{-2} \, \mathrm{cm}^3 \, \mu\mathrm{G}^{-1} \, \mathrm{pc}^{-1} = 2.6 \times 10^{-17} \, \mathrm{G}^{-1}$ being a constant. Evidently, Faraday depolarization is canceled if $\psi_P + \phi\lambda^2 = 0$.

In essence, for edge-on galaxies, we expect maximum polarized emission in diagonally opposite quadrants of a galaxy; see Fig. 19.12 of Ref. 31. This technique has also been applied to synthetic data of the solar corona.[32]

### 3.2.4. Magnetic helicity proxy

In the context of cosmology, a proxy of parity breaking and finite helicity of the cosmic microwave background and the Galactic foreground is obtained by decomposing the observed linear polarization in the sky into parity-even and parity-odd contributions. This is done by expanding the complex polarization $P \equiv Q + \mathrm{i}U$ with Stokes parameters $Q$ and $U$ into a spin-2 spherical harmonics as[33,34]

$$\tilde{R}_{\ell m} = \int_{4\pi} (Q + \mathrm{i}U) \, _2Y_{\ell m}^*(\theta, \phi) \, \sin\theta \, \mathrm{d}\theta \, \mathrm{d}\phi. \tag{9}$$

The parity-even ($E$) and parity-odd ($B$) contributions are obtained as the real and imaginary parts of the return transformation as[35,36]

$$E + \mathrm{i}B \equiv R = \sum_{\ell=2}^{N_\ell} \sum_{m=-\ell}^{\ell} \tilde{R}_{\ell m} Y_{\ell m}(\theta, \phi). \tag{10}$$

In cosmology, one usually considers correlations between $E$ and $B$, as well as temperature and $B$, for example. However, it is also useful to consider $B$ on its own, as was done in the context of the solar magnetic field[37] and in the context of the Galactic magnetic field.[38] The result for our Galaxy is shown in Figure 3.

We see that the $B$ polarization is locally antisymmetric about the equatorial plane, but there are canceling contributions from different longitudes, so the longitudinal average is much smaller. Nevertheless, even the longitudinal average does show a hemispheric antisymmetry.

Comparing with synthetic observations using the magnetic field from idealized dynamo models[39] shows that this hemispheric dependence does not originate from the different signs of the magnetic helicity expected in the northern and southern hemispheres, but from the spiral pattern of our Galaxy, where the views from the north and south correspond to mirror images of each other.
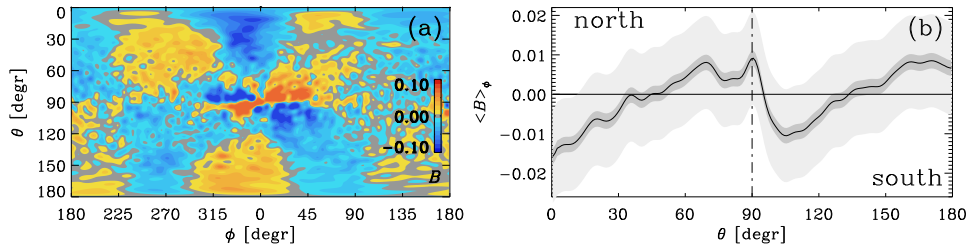
Fig. 3.   Left: Galactic $B$ mode polarization. Right: longitudinally averaged $B$ mode polarization. Here, $\theta$ and $\phi$ are Galactic colatitude ($= 90° -$ latitude) and longitude.

## 4. Magnetic helicity throughout the whole Universe

There is at present no definitive observation of finite helicity throughout all of the Universe, but the possibility certainly exists.[40] In this section, we first discuss two quite different mechanisms. One is related to the chiral magnetic effect (CME) and the other to inflationary magnetogenesis. Both generate helical magnetic fields, and the electromagnetic stress can generate relic gravitational waves (GWs) that are circularly polarized. Such waves, once generated, would not dissipate and would only dilute under the cosmic expansion. They could still be observable with space interferometers[41–43] and with pulsar timing arrays.[44] Measuring circular polarization could provide a clean mechanism for determining the sign of helicity in the Universe.

In the following, we describe the two generation mechanisms and compare in Figure 4 the growth of the resulting magnetic field and the circular polarization of GWs that could be observed in future using space interferometers in the millihertz range.[41–43]

### 4.1. *The CME*

The CME is a quantum effect associated with the systematic alignment of the spin $s$ of electrically charged fermions (electrons or positrons, for example) with the momentum $p$. A nonvanishing net helicity $s \cdot p$ originates from the parity-breaking weak force and manifests itself in the $\beta$ decay, for example, where spin and momentum of electrons are antialigned, i.e., $s \cdot p < 0$. The sign would be opposite for antimatter, i.e., for positrons, for example. However, at low energies, spin flipping occurs,[45] making this effect important only for highly relativistic plasmas at high enough temperatures.

In the presence of a magnetic field, the spin of chiral fermions aligns itself with the magnetic field, and, owing to the finite momentum and charge of the fermions, they produce a net current along the magnetic field,[46–50]

$$\boldsymbol{J} = 24\alpha_{\mathrm{em}} \left(n_{\mathrm{L}} - n_{\mathrm{R}}\right) \left(\frac{k_{\mathrm{B}}T}{\hbar c}\right)^2 \boldsymbol{B}, \qquad (11)$$
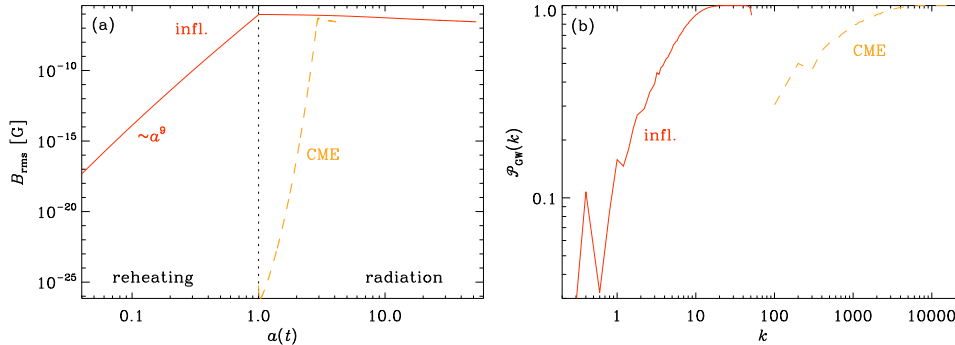
Fig. 4. (a) Growth of magnetic field from the CME (orange) and inflationary magnetogenesis (red), where time is here expressed in terms of the scale factor of the Universe $a(t)$, which increases monotonically and is set to unity at the beginning of the radiation-dominated era. Note the algebraic increase $B_{\rm rms} \propto a^9$. (b) Circular polarization spectra of GWs produced from the CME (orange) and inflationary magnetogenesis (red).

where $\alpha_{\rm em} \approx 1/137$ is the fine structure constant, $n_{\rm L}$ and $n_{\rm R}$ are the number densities of left- and right-handed fermions, respectively, $k_{\rm B}$ is the Boltzmann constant, $T$ is the temperature of the Universe today, $\hbar$ is the reduced Planck constant, and $c$ is the speed of light.

We see the analogy with Eq. (5), where we had a mean electromotive force $\overline{\boldsymbol{\mathcal{E}}} \equiv \overline{\boldsymbol{u} \times \boldsymbol{b}}$ with a mean current $\overline{\boldsymbol{J}} = (\alpha/\eta_{\rm t}\mu_0)\,\overline{\boldsymbol{B}}$ produced along the mean magnetic field for turbulent for helical turbulence. Similar to the dynamo effect in helical turbulence, there is a dynamo effect associated with chiral plasmas. This was discussed in the context of cosmology[47] as a mechanism for producing magnetic fields in the early Universe. This effect produces helical magnetic fields, and the associated helicity reduces the net chirality of the fermions such that the total chirality is conserved, i.e.,

$$(n_{\rm L} - n_{\rm R}) + \frac{4\alpha_{\rm em}}{\hbar c}\langle \boldsymbol{A} \cdot \boldsymbol{B}\rangle = \text{const.} \tag{12}$$

The length scales are small compared with the Hubble radius at any given time and the resulting field strengths are limited to[51]

$$|\langle \boldsymbol{A} \cdot \boldsymbol{B}\rangle| \lesssim \xi_{\rm M}\langle \boldsymbol{B}^2\rangle \lesssim (0.5 \times 10^{-18}\,{\rm G})^2\,{\rm Mpc}, \tag{13}$$

where $\xi_{\rm M}$ is the magnetic correlation length, measured here in megaparsec ($1\,{\rm Mpc} \approx 3 \times 10^{24}\,{\rm cm}$). This value of $\xi_{\rm M}\langle \boldsymbol{B}^2\rangle$ is below the lower limits derived from the non-observation of secondary GeV photons that are expected from inverse Compton scattering of TeV photons from energetic blazers. One can therefore not be very hopeful that those lower limits on the magnetic field can be explained as a result of the CME. However, stronger fields could still be produced during inflation, as will be discussed next.

### 4.2. *Inflationary magnetogenesis*

Models of inflationary magnetogenesis tend to invoke conformal invariance-breaking to generate magnetic fields as a result of stretching without diluting the magnetic energy during the inflationary expansion and the subsequent reheating phase when most of the relevant particles and photons were produced. Conformal invariance-breaking means that the term $F_{\mu\nu}F^{\mu\nu}$ in the Lagrangian density is replaced by $f^2 F_{\mu\nu}F^{\mu\nu}$ with $f \neq 1$ during inflation[52] and reheating.[53] In the presence of such a term, the vacuum evolution equation for the vector potential changes from a standard wave equation $(\partial^2/\partial t^2 + k^2)\tilde{\mathbf{A}} = 0$ to $(\partial^2/\partial t^2 + k^2 - f''/f)(f\tilde{\mathbf{A}}) = 0$, where $t$ is now conformal time and the primes on $f$ denote derivatives with respect to conformal time.

Commonly adopted forms of $f$ include $f \propto a^\alpha$ during inflation and $f \propto a^{-\beta}$ during reheating.[54–57]. In the presence of pseudoscalars $\gamma$, such as axions, one also expects terms of the form $\gamma f^2 F_{\mu\nu}\tilde{F}^{\mu\nu}$ in the Lagrangian density. The evolution equation for $\tilde{\mathbf{A}}$ takes then the form

$$\left( \frac{\partial^2}{\partial t^2} + k^2 \pm 2\gamma k\frac{f'}{f} - \frac{f''}{f} \right)(f\tilde{A}_\pm) = 0, \tag{14}$$

where $\tilde{\mathbf{A}} = \tilde{A}_+\hat{\boldsymbol{e}}_+ + \tilde{A}_-\hat{\boldsymbol{e}}_-$ has been expressed in terms of the polarization basis $\tilde{\mathbf{e}}_\pm(\boldsymbol{k}) = [\tilde{\mathbf{e}}_1(\boldsymbol{k}) \pm \mathrm{i}\tilde{\mathbf{e}}_2(\boldsymbol{k})]/\sqrt{2}\,\mathrm{i}$ with $\mathrm{i}\boldsymbol{k} \times \tilde{\mathbf{e}}_\pm = \pm k\tilde{\mathbf{e}}_\pm$, and $\tilde{\mathbf{e}}_1(\boldsymbol{k})$, $\tilde{\mathbf{e}}_2(\boldsymbol{k})$ represent units vectors orthogonal to $\boldsymbol{k}$ and orthogonal to each other. Figure 4(a) shows the resulting algebraic growth of the magnetic field in comparison with the exponential growth from the CME, and panel (b) shows the circular polarization spectrum $\mathcal{P}_{\mathrm{GW}}(k)$. It is defined as[58]

$$\mathcal{P}_{\mathrm{GW}}(k) = \int 2\,\mathrm{Im}\,\tilde{h}_+\tilde{h}_\times^*\, k^2 \mathrm{d}\Omega_k \bigg/ \int \left( |\tilde{h}_+|^2 + |\tilde{h}_\times|^2 \right) k^2 \mathrm{d}\Omega_k. \tag{15}$$

We see that the degree of polarization reaches nearly 100% in a certain range.[59,60]

### 4.3. *Detecting handedness from unit vectors in the sky*

In addition to measuring the polarization of GWs as an indicator of the helicity of the underlying magnetic field, there is yet another interesting method that we describe here briefly. Suppose we observed energetic photons from a particular astrophysical source from three slightly different directions, $\hat{\boldsymbol{n}}_1$, $\hat{\boldsymbol{n}}_2$, and $\hat{\boldsymbol{n}}_3$, and that their energies $E_i$ are ordered such that $E_1 < E_2 < E_3$, then we can construct a pseudoscalar

$$Q = (\hat{\boldsymbol{n}}_1 \times \hat{\boldsymbol{n}}_2) \cdot \hat{\boldsymbol{n}}_3. \tag{16}$$

The quantity $Q$ would change sign in a mirror image of our Universe. The value of $Q$ may well be zero within error bars, but if it is not, its sign must mean something.

Detailed calculations have shown the TeV photons from blazars (i.e., the accretion disk around supermassive black holes) can upscatter on the cosmic background

12

light and produce GeV photons.[61] Using about 10,000 photons observed with Fermi Large Area Telescope data over a period of about five years, Tashiro et al.[62] found $Q < 0$ for all possible photon triples in certain energy ranges. They interpreted this as evidence in favor of a baryogenesis scenario that proceeds through changes in the Chern-Simons number, which implies the generation of magnetic fields of negative helicity;[63] see also Ref. 64 for a review.

In all the studies of $Q$ done since then,[65–68] one introduced a cutoff toward low Galactic latitudes so as to avoid excess contamination from our Galaxy. Using synthetic data, it has been found[69] that it is this procedure that leads to the occurrence of large statistical errors in the estimate of $Q$. Updated observations covering 11 years turned out to be no longer compatible with a detection of a negative value of $Q$.[69] This has been confirmed in subsequent work.[70] Thus, although this method could work in principle, it would require much better statistics.

In this connection, it is interesting to note that an equivalent quantity $Q$ can be determined for a variety of different observations. Suppose there are three sunspots of different strengths on the surface of the Sun, this again implies a finite handedness. We can then ask whether this handedness could be linked to the helicity of the underlying magnetic field. Idealized model calculations have shown that this is indeed the case.[71]

## 5. Spontaneous chirality production

### 5.1. *Biological homochirality*

In astrobiology, an important question concerns the origin of biological homochirality.[72] In solution, many organic molecules tend to rotate the polarization plane of linearly polarized light. One refers to the substances as either levorotatory (L for left-handed) or dextrorotatory (D for right-handed). Almost all amino acids of terrestrial life are of the L form, and almost all sugars are of the D form, for example the sugars in the phosphorus backbones of deoxyribose nucleic acid (DNA). The origin of this homochirality can be explained in terms of two essential processes: autocatalysis and mutual antagonism – an old idea that goes back to a paper by F. C. Frank[73] of 1953. Interestingly, this is the same year when Watson and Crick[74] discovered the helix structure of DNA.

Autocatalysis produces "more of itself", i.e., it can catalyze the formation of chiral molecules of the L form from an achiral substrate $A$ in the presence of L and, conversely, it can catalyze the formation of molecules of the D form in the presence of D. The corresponding reactions

$$L + A \rightarrow 2L \quad \text{and} \quad D + A \rightarrow 2D, \tag{17}$$
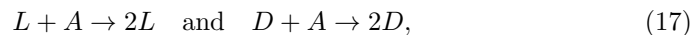
with rate coefficient $k_{\mathrm{C}}$, imply that the associated concentrations $[L]$ and $[D]$ obey

$$\frac{\mathrm{d}}{\mathrm{d}t}[L] = k_{\mathrm{C}}[A][L] - ... \quad \text{and} \quad \frac{\mathrm{d}}{\mathrm{d}t}[D] = k_{\mathrm{C}}[A][D] - ..., \tag{18}$$

which leads to exponential growth with time $t$ of both $[L] = [L]_0 e^{k_C[A]t}$ and $[D] = [D]_0 e^{k_C[A]t}$, with initial values $[L]_0$ and $[D]_0$. However, this process alone does not change the enantiomeric excess (e.e.), e.e. $= ([L]-[D])/([L]+[D])$, which will always be equal to the initial value. This is because we still need mutual antagonism, which will be explained next.

For a long time, it remained unclear what would correspond to Frank's mutual antagonism. The relevant understanding was put forward by Sandars.[75] At that time, it was thought that homochirality was a prerequisite to the origin of life. This idea was based on an experimental result by Joyce et al.,[76] which showed that in template-directed polymerization of oligomers of one chirality, polymers of the opposite chirality terminate further polymerization. This was called enantiomeric cross-inhibition, and was regarded as a serious problem for the origin of life, and that life could only emerge in a fully homochiral environment.[77] Sandars realized that enantiomeric cross-inhibition could just be the crucial mechanism that corresponds to Frank's mutual antagonism that would lead to the emergence of homochirality. The corresponding reaction and rate equations, with rate coefficient $k_I$, are

$$L + D \to 2A \quad \text{and} \quad \frac{\mathrm{d}}{\mathrm{d}t}[A] = 2k_I[L][D] - \dots . \tag{19}$$
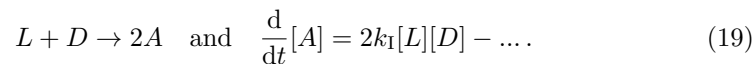
Multiple extensions of Sanders' model have been produced[78–81] and there are also other variants that are not based on nucleotides, but on peptides.[82–85] If one regards these first polymerization reactions as the first steps toward life, one could then say that homochirality emerges as a consequence of life, and not as a prerequisite.[86,87]

The lessons learnt from astrobiology may well be applicable to other fields of physics, and in particular to MHD. Examples were found in the context of the magnetobuoyancy instability[88] and the Tayler instability.[89,90] In those cases, there are two unstable eigenfunctions that are helical and have positive and negative helicities, respectively, but their growth rates are equal. This process corresponds to autocatalysis. The nonlinearity in the MHD equations, associated with the Lorentz force, corresponds to mutual antagonism. The resulting amplitude equations in MHD are the same as in the production of homochirality.[90] Another more recent example of this type has been found in studies of the CME when the chiral chemical potential is fluctuating around zero.[91,92] Again, one chirality becomes eventually dominant, and this choice depends on details in the initial conditions.

## 5.2. *Spatially distinct domains of chirality*

In spatially extended domains, the evolution equations for $[L]$ and $[D]$ attain additional spatial diffusion terms and become then similar to the Fisher equation[93] which describes front propagation. In the present case, once fronts of L and D polymers come into contact, the front between them comes to a halt and cannot propagate any further, unless the front is curved. If it is curved, the front continues
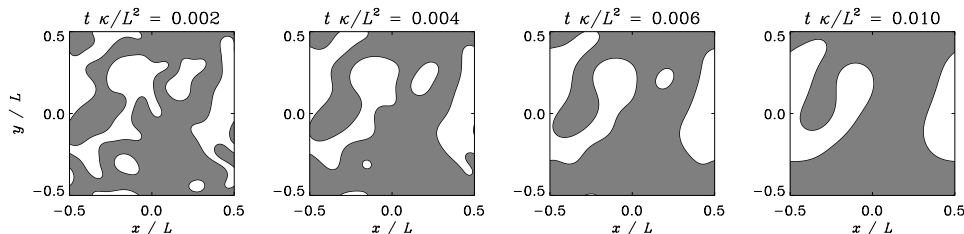
14



Fig. 5.   Gradual shrinking of isolated islands on one handedness (white), leading to the eventual dominance of the other (gray).
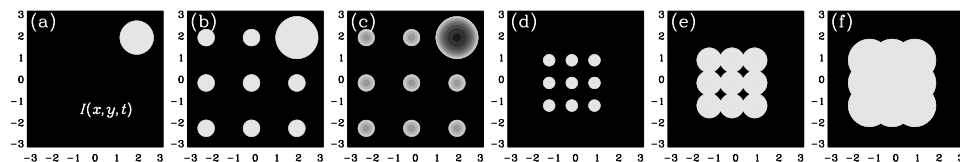


Fig. 6.   The number of infected $I(x,y)$ in a two-dimensional Cartesian plane $(x,y)$, as obtained from model calculations,[95] showing (a) a circular spreading center in the upper right corner, (b) the subsequent emergence of eight additional spreading centers that (c) continue to grow, but with decreasing $I(x,y)$ in their centers due to recovery or death. Note that the total length of the periphery increases when the number of spreading centers increases.  Panels (d)–(f) show a case where spreading centers merge, so the growth in the length of the periphery declines.

to propagate in the direction of largest curvature.[94] This leads in the end to small near-circular islands that shrink until they disappear; see Figure 5.  This means that the enantiomeric excess changes in a piecewise linear fashion.

## 5.3.  *Analogous mechanisms in other systems*

Given that closed patches of one handedness always shrink and eventually disappear, it is clear that the dominant chirality must in the end be that of the outside of the last surviving patch. Thus, it is not necessarily the one that was initially the most dominant one.

A piecewise linear evolution is common to many spatially extended systems, including those describing the spread of SARS-CoV-2 over the past two years. Here, however, it is not the number $N$ itself, but its square root, $N^{1/2}$. In Figure 6, we show the spatial geometry of a hypothetic spreading center in the upper right corner. The speed of growth depends just on the length of the periphery. At a later time, there will be new spreading centers, so the total length of the periphery increases. This happened in the middle of March 2020; see Figure 7. During the first part of the epidemic (denoted by a red A), the evolution was comparatively slow and the disease was essentially confined just to China. During the subsequent phase (denoted by a blue B) it spread all over the world. This led to an increase in the
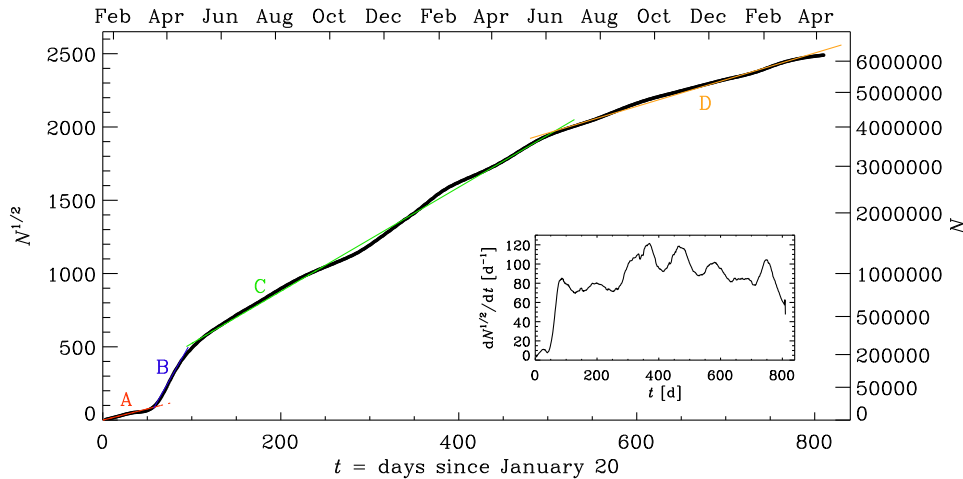
Fig. 7.  Square root of the number $N$ of deaths, which is regarded as a proxy of the number of infected that is more reliable than the reported number of SARS-CoV-2.  Note the piecewise linear growth in $N^{1/2}$, corresponding to a piecewise quadratic growth.  The line segments A–D are described in the text.

total length of the periphery.  Later, different spreading centers began to emerge, so the total periphery has now decreased again, and the growth has slowed down (denoted by the green and orange segments C and D, respectively), but it always remained piecewise quadratic and was never exponential.[95]  The spreading of SARS-CoV-2 is obviously no longer directly related to the topic of chirality in astrophysics, but it is interesting to see that the mathematics of front propagation in spatially extended domains is similar to that of left and right handed life forms invading the early Earth.[94]

## 6.  Conclusions

In this work, we have sketched three rather different ways of achieving chirality in astrophysics and astrobiology: externally driven, intrinsically driven, and spontaneous chirality production.  The first two mechanisms are particularly relevant to fluid dynamics and magnetic fields, while the last one of spontaneous chirality production is mainly relevant to astrobiology and to the origin of life, but it remains hypothetic until one is able to find an example of another genesis of life independent of that on Earth, for example on Mars or on some of the icy moons in our solar system.[72]

The idea of propagating fronts of life forms of opposite handedness is intriguing and it would be useful to reproduce this in the lab.  This may not be easy because such fronts propagate relatively rapidly under laboratory conditions.  In fact, their propagation resembles the propagation of epidemiological fronts, such as the black death[96] and perhaps even SARS-CoV-2.[95]  However, the application to the early

16

Earth implies much larger spatial scales. Earlier work quoted half a billion years as a relevant time scale.[94] However, if one thinks of the deep biosphere of Mars, it may not be impossible to explain a possible detection of opposite chiralities of DNA, if such should ever be observed on Mars or in its permafrost.

Alternatively, it is possible that the chirality of biomolecules is determined through an external influence.[97] Such an influence would then, similarly to the intrinsically driven chirality discussed in Sect. 4, be related to the parity-breaking weak force. This possibility cannot easily be dismissed. In particular, a 2% enantiomeric excess in favor of the L form has been found for amino acids in the Murchison meteorite.[98] This was a pristine meteorite rich in organics, as already evidenced by the smell reported by initial eyewitnesses. On the other hand, those molecules are also susceptible to contamination, while those not susceptible to contamination did not show any enantiomeric excess.

Determining a global chirality that is the same throughout the entire Universe would be a major discovery. Measuring the chirality through circular polarization of GWs would likely be the most definitive proof of parity violation in the Universe.

### Acknowledgments

### References

1. H. K. Moffatt, The degree of knottedness of tangled vortex lines, *J. Fluid Mech.* **35**, 117 (1969).
2. R. Betchov, Semi-Isotropic Turbulence and Helicoidal Flows, *Physics of Fluids* **4**, 925 (July 1961).
3. L. Woltjer, A theorem on force-free magnetic fields, *Proc. Nat. Acad. Sci.* **44**, 489 (1958).
4. J. B. Taylor, Relaxation of Toroidal Plasma and Generation of Reverse Magnetic Fields, *Phys. Rev. Lett.* **33**, 1139 (November 1974).
5. A. Brandenburg and K. Subramanian, Astrophysical magnetic fields and nonlinear dynamo theory, *Phys. Rep.* **417**, 1 (2005).
6. F. Krause and K.-H. Rädler, *Mean-Field Magnetohydrodynamics and Dynamo Theory* (Pergamon Press (also Akademie-Verlag: Berlin), Oxford, 1980).
7. A. Brandenburg, The inverse cascade and nonlinear alpha-effect in simulations of isotropic helical hydromagnetic turbulence, *Astrophys. J.* **550**, 824 (2001).
8. F. Rincon, Dynamo theories, *J. Plasma Phys.* **85**, 205850401 (2019).

9.  H. Zhang and A. Brandenburg, Solar kinetic energy and cross helicity spectra, *Astrophys. J. Lett.* **862**, L17 (2018).

10. G. Rüdiger, L. L. Kitchatinov and A. Brandenburg, Cross helicity and turbulent magnetic diffusivity in the solar convection zone, *Sol. Phys.* **269**, 3 (2011).

11. A. Brandenburg, N. Kleeorin and I. Rogachevskii, Self-assembly of shallow magnetic spots through strongly stratified turbulence, *Astrophys. J. Lett.* **776**, L23 (2013).

12. A. Brandenburg, O. Gressel, S. Jabbari, N. Kleeorin and I. Rogachevskii, Mean-field and direct numerical simulations of magnetic flux concentrations from vertical field, *Astron. Astrophys.* **562**, A53 (2014).

13. P. Demoulin and E. R. Priest, A twisted flux model for solar prominences. II - Formation of a dip in a magnetic structure before the formation of a solar prominence, *Astron. Astrophys.* **214**, 360 (1989).

14. S. E. Gibson, L. Fletcher, G. Del Zanna, C. D. Pike, H. E. Mason, C. H. Mandrini, P. Démoulin, H. Gilbert, J. Burkepile, T. Holzer, D. Alexander, Y. Liu, N. Nitta, J. Qiu, B. Schmieder and B. J. Thompson, The structure and evolution of a sigmoidal active region, *Astrophys. J.* **574**, 1021 (2002).

15. Y. Guo, M. D. Ding, X. Cheng, J. Zhao and E. Pariat, Twist accumulation and topology structure of a solar magnetic flux rope, *Astrophys. J.* **779**, 157 (2013).

16. M. K. Georgoulis, A new technique for a routine azimuth disambiguation of solar vector magnetograms, *Astrophys. J. Lett.* **629**, L69 (2005).

17. G. V. Rudenko and S. A. Anfinogentov, Very fast and accurate azimuth disambiguation of vector magnetograms, *Sol. Phys.* **289**, 1499 (2014).

18. N. Seehafer, Electric current helicity in the solar atmosphere, *Sol. Phys.* **125**, 219 (1990).

19. H. Zhang, A. Brandenburg and D. D. Sokoloff, Magnetic helicity and energy spectra of a solar active region, *Astrophys. J. Lett.* **784**, L45 (2014).

20. H. Zhang, A. Brandenburg and D. D. Sokoloff, Evolution of magnetic helicity and energy spectra of solar active regions, *Astrophys. J.* **819**, 146 (2016).

21. W. H. Matthaeus, M. L. Goldstein and C. Smith, Evaluation of magnetic helicity in homogeneous turbulence, *Phys. Rev. Lett.* **48**, 1256 (May 1982).

22. A. Brandenburg, K. Subramanian, A. Balogh and M. L. Goldstein, Scale dependence of magnetic helicity in the solar wind, *Astrophys. J.* **734**, 9 (2011).

23. A. Brandenburg, S. Candelaresi and P. Chatterjee, Small-scale magnetic helicity losses from a mean-field dynamo, *Mon. Not. Roy. Astron. Soc.* **398**, 1414 (2009).

24. J. Warnecke, A. Brandenburg and D. Mitra, Dynamo-driven plasmoid ejections above a spherical surface, *Astron. Astrophys.* **534**, A11 (2011).

25. J. Warnecke, A. Brandenburg and D. Mitra, Magnetic twist: a source and property of space weather, *J. Space Weather Space Climate* **2**, A260000 (2012).

26. J.-Z. Zhu, W. Yang and G.-Y. Zhu, Purely helical absolute equilibria and chirality of (magneto)fluid turbulence, *Journal of Fluid Mechanics* **739**, 479 (January 2014).

27. J.-Z. Zhu, Chirality, extended magnetohydrodynamics statistics and topological constraints for solar wind turbulence, *Mon. Not. Roy. Astron. Soc.* **470**, L87 (June 2017).

28. Y. Narita, G. Kleindienst and K. H. Glassmeier, Evaluation of magnetic helicity density in the wave number domain using multi-point measurements in space, *Annales Geophysicae* **27**, 3967 (October 2009).

29. A. Brandenburg and R. Stepanov, Faraday signature of magnetic helicity from reduced depolarization, *Astrophys. J.* **786**, 91 (2014).

30. C. Horellou and A. Fletcher, Magnetic field tomography, helical magnetic fields and Faraday depolarization, *Mon. Not. Roy. Astron. Soc.* **441**, 2049 (2014).

31. A. Brandenburg, Simulations of galactic dynamos, *Astrophys. Spa. Sci. Lib.* **407**, 529

18

(2015).

32. A. Brandenburg, M. B. Ashurova and S. Jabbari, Compensating Faraday depolarization by magnetic helicity in the solar corona, *Astrophys. J.* **845**, L15 (2017).
33. M. Kamionkowski, A. Kosowsky and A. Stebbins, A probe of primordial gravity waves and vorticity, *Phys. Rev. Lett.* **78**, 2058 (1997).
34. U. Seljak and M. Zaldarriaga, Signature of gravity waves in the polarization of the microwave background, *Phys. Rev. Lett.* **78**, 2054 (1997).
35. R. Durrer, *The Cosmic Microwave Background* (Cambridge University Press, Cambridge, 2008).
36. M. Kamionkowski and E. D. Kovetz, The quest for B modes from inflationary gravitational waves, *Ann. Rev. Astron. Astrophys.* **54**, 227 (2016).
37. A. Brandenburg, A global two-scale helicity proxy from $\pi$-ambiguous solar magnetic fields, *Astrophys. J.* **883**, 119 (2019).
38. A. Brandenburg and M. Brüggen, Hemispheric handedness in the Galactic synchrotron polarization foreground, *Astrophys. J. Lett.* **896**, L14 (2020).
39. A. Brandenburg and R. S. Furuya, Application of a helicity proxy to edge-on galaxies, *Mon. Not. Roy. Astron. Soc.* **496**, 4749 (2020).
40. T. Vachaspati, Estimate of the primordial magnetic field helicity, *Phys. Rev. Lett.* **87**, 251302 (2001).
41. C. Caprini, M. Hindmarsh, S. Huber, T. Konstandin, J. Kozaczuk, G. Nardini, J. M. No, A. Petiteau, P. Schwaller, G. Servant and D. J. Weir, Science with the space-based interferometer eLISA. II: gravitational waves from cosmological phase transitions, *J. Cosm. Astropart. Phys.* **2016**, 001 (2016).
42. P. Amaro-Seoane, H. Audley, S. Babak, J. Baker, E. Barausse, P. Bender, E. Berti, P. Binetruy, M. Born, D. Bortoluzzi, J. Camp, C. Caprini, V. Cardoso, M. Colpi, J. Conklin, N. Cornish, C. Cutler, K. Danzmann, R. Dolesi, L. Ferraioli, V. Ferroni, E. Fitzsimons, J. Gair, L. Gesa Bote, D. Giardini, F. Gibert, C. Grimani, H. Halloin, G. Heinzel, T. Hertog, M. Hewitson, K. Holley-Bockelmann, D. Hollington, M. Hueller, H. Inchauspe, P. Jetzer, N. Karnesis, C. Killow, A. Klein, B. Klipstein, N. Korsakova, S. L. Larson, J. Livas, I. Lloro, N. Man, D. Mance, J. Martino, I. Mateos, K. McKenzie, S. T. McWilliams, C. Miller, G. Mueller, G. Nardini, G. Nelemans, M. Nofrarias, A. Petiteau, P. Pivato, E. Plagnol, E. Porter, J. Reiche, D. Robertson, N. Robertson, E. Rossi, G. Russano, B. Schutz, A. Sesana, D. Shoemaker, J. Slutsky, C. F. Sopuerta, T. Sumner, N. Tamanini, I. Thorpe, M. Troebs, M. Vallisneri, A. Vecchio, D. Vetrugno, S. Vitale, M. Volonteri, G. Wanner, H. Ward, P. Wass, W. Weber, J. Ziemer and P. Zweifel, Laser Interferometer Space Antenna, *arXiv e-prints* , p. arXiv:1702.00786 (2017).
43. Y.-L. Taiji Scientific Collaboration, Wu, Z.-R. Luo, J.-Y. Wang, M. Bai, W. Bian, R.-G. Cai, Z.-M. Cai, J. Cao, D.-J. Chen, L. Chen, L.-S. Chen, M.-W. Chen, W.-B. Chen, Z.-Y. Chen, L.-X. Cong, J.-F. Deng, X.-L. Dong, L. Duan, S.-Q. Fan, S.-S. Fan, C. Fang, Y. Fang, K. Feng, P. Feng, Z. Feng, R.-H. Gao, R.-L. Gao, Z.-K. Guo, J.-W. He, J.-B. He, X. Hou, L. Hu, W.-R. Hu, Z.-Q. Hu, M.-J. Huang, J.-J. Jia, K.-L. Jiang, G. Jin, H.-B. Jin, Q. Kang, J.-G. Lei, B.-Q. Li, D.-J. Li, F. Li, H.-S. Li, H.-W. Li, L.-F. Li, W. Li, X.-K. Li, Y.-M. Li, Y.-G. Li, Y.-P. Li, Y.-P. Li, Z. Li, Z.-Y. Lin, C. Liu, D.-B. Liu, H.-S. Liu, H. Liu, P. Liu, Y.-R. Liu, Z.-Y. Lu, H.-W. Luo, F.-L. Ma, L.-F. Ma, X.-S. Ma, X. Ma, Y.-C. Man, J. Min, Y. Niu, J.-K. Peng, X.-D. Peng, K.-Q. Qi, L.-É. Qiang, C.-F. Qiao, Y.-X. Qu, W.-H. Ruan, W. Sha, J. Shen, X.-J. Shi, R. Shu, J. Su, Y.-L. Sui, G.-W. Sun, W.-L. Tang, H.-J. Tao, W.-Z. Tao, Z. Tian, L.-F. Wan, C.-Y. Wang, J. Wang, J. Wang, L.-L. Wang, S.-X. Wang, X.-P. Wang, Y.-K. Wang, Z. Wang, Z.-L. Wang, Y.-X. Wei, L.-M. Di Wu, Wu, P.-Z. Wu, Z.-H. Wu,

D.-X. Xi, Y.-F. Xie, G.-F. Xin, L.-X. Xu, P. Xu, S.-Y. Xu, Y. Xu, S.-W. Xue, Z.-B. Xue, C. Yang, R. Yang, S.-J. Yang, S. Yang, Y. Yang, Z.-G. Yang, Y.-L. Yin, J.-P. Yu, T. Yu, À.-B. Zhang, C. Zhang, M. Zhang, X.-Q. Zhang, Y.-Z. Zhang, J. Zhao, W.-W. Zhao, Y. Zhao, J.-H. Zheng, C.-Y. Zhou, Z.-C. Zhu, X.-B. Zou and Z.-M. Zou, China's first step towards probing the expanding universe and the nature of gravity using a space borne gravitational wave antenna, *CmPhy* **4**, 34 (2021).

44. Z. Arzoumanian, P. T. Baker, H. Blumer, B. Bécsy, A. Brazier, P. R. Brook, S. Burke-Spolaor, S. Chatterjee, S. Chen, J. M. Cordes, N. J. Cornish, F. Crawford, H. T. Cromartie, M. E. Decesar, P. B. Demorest, T. Dolch, J. A. Ellis, E. C. Ferrara, W. Fiore, E. Fonseca, N. Garver-Daniels, P. A. Gentile, D. C. Good, J. S. Hazboun, A. M. Holgado, K. Islo, R. J. Jennings, M. L. Jones, A. R. Kaiser, D. L. Kaplan, L. Z. Kelley, J. S. Key, N. Laal, M. T. Lam, T. J. W. Lazio, D. R. Lorimer, J. Luo, R. S. Lynch, D. R. Madison, M. A. McLaughlin, C. M. F. Mingarelli, C. Ng, D. J. Nice, T. T. Pennucci, N. S. Pol, S. M. Ransom, P. S. Ray, B. J. Shapiro-Albert, X. Siemens, J. Simon, R. Spiewak, I. H. Stairs, D. R. Stinebring, K. Stovall, J. P. Sun, J. K. Swiggum, S. R. Taylor, J. E. Turner, M. Vallisneri, S. J. Vigeland, C. A. Witt and Nanograv Collaboration, The NANOGrav 12.5 yr data set: Search for an isotropic stochastic gravitational-wave background, *Astrophys. J. Lett.* **905**, L34 (2020).

45. A. Boyarsky, V. Cheianov, O. Ruchayskiy and O. Sobol, Evolution of the primordial axial charge across cosmic times, *Phys. Rev. Lett.* **126**, 021801 (2021).

46. A. Vilenkin, Equilibrium parity-violating current in a magnetic field, *Phys. Rev. D* **22**, 3080 (1980).

47. M. Joyce and M. Shaposhnikov, Primordial magnetic fields, right electrons, and the Abelian anomaly, *Phys. Rev. Lett.* **79**, 1193 (1997).

48. A. Boyarsky, J. Fröhlich and O. Ruchayskiy, Self-consistent evolution of magnetic fields and chiral asymmetry in the early Universe, *Phys. Rev. Lett.* **108**, 031301 (2012).

49. A. Boyarsky, J. Fröhlich and O. Ruchayskiy, Magnetohydrodynamics of chiral relativistic fluids, *Phys. Rev. D* **92**, 043004 (2015).

50. I. Rogachevskii, O. Ruchayskiy, A. Boyarsky, J. Fröhlich, N. Kleeorin, A. Brandenburg and J. Schober, Laminar and turbulent dynamos in chiral magnetohydrodynamics. I. Theory, *Astrophys. J.* **846**, 153 (2017).

51. A. Brandenburg, J. Schober, I. Rogachevskii, T. Kahniashvili, A. Boyarsky, J. Fröhlich, O. Ruchayskiy and N. Kleeorin, The turbulent chiral magnetic cascade in the early Universe, *Astrophys. J.* **845**, L21 (2017).

52. B. Ratra, Cosmological "Seed" Magnetic Field from Inflation, *Astrophys. J. Lett.* **391**, L1 (1992).

53. V. Demozzi and C. Ringeval, Reheating constraints in inflationary magnetogenesis, *J. Cosm. Astropart. Phys.* **2012**, 009 (2012).

54. R. J. Z. Ferreira, R. K. Jain and M. S. Sloth, Inflationary magnetogenesis without the strong coupling problem, *J. Cosm. Astropart. Phys.* **2013**, 004 (2013).

55. R. Sharma, S. Jagannathan, T. R. Seshadri and K. Subramanian, Challenges in inflationary magnetogenesis: Constraints from strong coupling, backreaction, and the Schwinger effect, *Phys. Rev. D* **96**, 083511 (2017).

56. R. Sharma, K. Subramanian and T. R. Seshadri, Generation of helical magnetic field in a viable scenario of inflationary magnetogenesis, *Phys. Rev. D* **97**, 083503 (2018).

57. A. Brandenburg and R. Sharma, Simulating relic gravitational waves from inflationary magnetogenesis, *Astrophys. J.* **920**, 26 (2021).

58. A. Roper Pol, A. Brandenburg, T. Kahniashvili, A. Kosowsky and S. Mandal, The timestep constraint in solving the gravitational wave equations sourced by hydromagnetic turbulence, *Geophys. Astrophys. Fluid Dynam.* **114**, 130 (2020).

20

59. A. Brandenburg, Y. He, T. Kahniashvili, M. Rheinhardt and J. Schober, Relic Grav-
    itational Waves from the Chiral Magnetic Effect, *Astrophys. J.* **911**, 110 (2021).
60. A. Brandenburg, Y. He and R. Sharma, Simulations of Helical Inflationary Magneto-
    genesis and Gravitational Waves, *Astrophys. J.* **922**, p. 192 (December 2021).
61. H. Tashiro and T. Vachaspati, Cosmological magnetic field correlators from blazar
    induced cascade, *Phys. Rev. D* **87**, 123527 (2013).
62. H. Tashiro, W. Chen, F. Ferrer and T. Vachaspati, Search for CP violating signature
    of intergalactic magnetic helicity in the gamma-ray sky., *Mon. Not. Roy. Astron. Soc.*
    **445**, L41 (2014).
63. T. Vachaspati, Estimate of the primordial magnetic field helicity, *Phys. Rev. Lett.* **87**,
    251302 (2001).
64. T. Vachaspati, Progress on cosmological magnetic fields, *Rep. Prog. Phys.* (2021).
65. W. Chen, J. H. Buckley and F. Ferrer, Search for GeV $\gamma$-ray pair halos around low
    redshift blazars, *Phys. Rev. Lett.* **115**, 211103 (2015).
66. W. Chen, B. D. Chowdhury, F. Ferrer, H. Tashiro and T. Vachaspati, Intergalactic
    magnetic field spectra from diffuse gamma-rays, *Mon. Not. Roy. Astron. Soc.* **450**,
    3371 (2015).
67. A. J. Long and T. Vachaspati, Morphology of blazar-induced gamma ray halos due to
    a helical intergalactic magnetic field, *J. Cosm. Astropart. Phys.* **2015**, 065 (2015).
68. A. J. Long and T. Vachaspati, Implications of a primordial magnetic field for magnetic
    monopoles, axions, and Dirac neutrinos, *Phys. Rev. D* **91**, 103522 (2015).
69. J. Asplund, G. Jóhannesson and A. Brandenburg, On the measurement of handedness
    in Fermi Large Area Telescope data, *Astrophys. J.* **898**, 124 (2020).
70. M. Kachelrieß and B. C. Martinez, Searching for primordial helical magnetic fields,
    *Phys. Rev. D* **102**, 083001 (2020).
71. P.-A. Bourdin and A. Brandenburg, Magnetic helicity from multipolar regions on the
    solar surface, *Astrophys. J.* **869**, 3 (2018).
72. D. Rothery, I. Gilmour and M. Sephton, *An Introduction to Astrobiology* (Cambridge
    University Press, 2011).
73. F. C. Frank, On spontaneous asymmetric synthesis, *Biochim. Biophys. Acta* **11**, 459
    (1953).
74. J. D. Watson and F. H. C. Crick, Molecular structure of nucleic acids: a structure for
    deoxyribose nucleic acid, *Nature* **171**, 737 (1953).
75. P. G. H. Sandars, A Toy Model for the Generation of Homochirality during Polymer-
    ization, *Orig. Life Evol. Biosph.* **33**, 575 (2003).
76. G. F. Joyce, G. M. Visser, C. A. A. van Boeckel, J. H. van Boom, L. E. Orgel and
    J. van Westrenen, Chiral selection in poly(C)-directed synthesis of oligo(G), *Nature*
    **310**, 602 (1984).
77. V. I. Gol'danskiĭ and V. V. Kuz'min, Spontaneous breaking of mirror symmetry in
    nature and the origin of life, *Soviet Physics Uspekhi* **32**, 1 (1989).
78. Y. Saito and H. Hyuga, Chirality selection in open flow systems and in polymerization,
    *Journal of the Physical Society of Japan* **74**, 1629 (2005).
79. A. Brandenburg, A. C. Andersen, S. Höfner and M. Nilsson, Homochiral growth
    through enantiomeric cross-inhibition, *Orig. Life Evol. Biosph.* **35**, 225 (2005).
80. J. A. D. Wattis and P. V. Coveney, Symmetry-breaking in chiral polymerisation, *Orig.
    Life Evol. Biosph.* **35**, 243 (2005).
81. M. Gleiser and S. I. Walker, An extended model for the evolution of prebiotic ho-
    mochirality: a bottom-up approach to the origin of life, *Orig. Life Evol. Biosph.* **38**,
    293 (2008).
82. R. Plasson, H. Bersini and A. Commeyras, Recycling Frank: Spontaneous emergence

of homochirality in noncatalytic systems, *Proc. Nat. Acad. Sci.* **101**, 16733 (2004).

83. A. Brandenburg, H. J. Lehto and K. M. Lehto, Homochirality in an early peptide world, *Astrobiology* **7**, 725 (2007).

84. M. Gleiser and S. I. Walker, Toward homochiral protocells in noncatalytic peptide systems, *Orig. Life Evol. Biosph.* **39**, 479 (2009).

85. K. K. Konstantinov and A. F. Konstantinova, Chiral symmetry breaking in large peptide systems, *Orig. Life Evol. Biosph.* **50**, 99 (2020).

86. P. G. H. Sandars, Chirality in the RNA world and beyond, *International Journal of Astrobiology* **4**, 49 (2005).

87. A. Brandenburg, Homochirality: a prerequisite or consequence of life?, in *Prebiotic Chemistry and the Origin of Life*, eds. A. Neubeck, and S. McMahon (Springer, 2021).

88. P. Chatterjee, D. Mitra, A. Brandenburg and M. Rheinhardt, Spontaneous chiral symmetry breaking by hydromagnetic buoyancy, *Phys. Rev. E* **84**, 025403 (2011).

89. M. Gellert, G. Rüdiger and R. Hollerbach, Helicity and $\alpha$-effect by current-driven instabilities of helical magnetic fields, *Mon. Not. Roy. Astron. Soc.* **414**, 2696 (2011).

90. A. Bonanno, A. Brandenburg, F. Del Sordo and D. Mitra, Breakdown of chiral symmetry during saturation of the Tayler instability, *Phys. Rev. E* **86**, 016313 (2012).

91. J. Schober, I. Rogachevskii and A. Brandenburg, Production of a Chiral Magnetic Anomaly with Emerging Turbulence and Mean-Field Dynamo Action, *Phys. Rev. Lett.* **128**, p. 065002 (February 2022).

92. J. Schober, I. Rogachevskii and A. Brandenburg, Dynamo instabilities in plasmas with inhomogeneous chiral chemical potential, *Phys. Rev. D* **105**, p. 043507 (February 2022).

93. R. A. Fisher, The wave of advance of advantageous genes, *Ann. Eugenics* **7**, 353 (1937).

94. A. Brandenburg and T. Multamäki, How long can left and right handed life forms coexist?, *Int. J. Astrobiology* **3**, 209 (2004).

95. A. Brandenburg, Piecewise quadratic growth during the 2019 novel coronavirus epidemic, *Infectious Disease Modelling* **5**, 681 (2020).

96. J. V. Noble, Geographic and temporal development of plagues, *Nature* **250**, 726 (1974).

97. N. Globus and R. D. Blandford, The chiral puzzle of life, *Astrophys. J. Lett.* **895**, L11 (2020).

98. S. Pizzarello and J. R. Cronin, Non-racemic amino acids in the Murray and Murchison meteorites, *Geochim. Cosmochim. Acta* **64**, 329 (2000).